Vibrational Normal Modes and Dynamical Stability of DNA Triplex Poly(dA) · 2Poly(dT): S-Type Structure Is More Stable and in Better Agreement with Observations in Solution

Y. Z. Chen,* J. W. Powell,# and E. W. Prohofsky*
*Department of Physics, Purdue University, West Lafayette, Indiana 47907-1396, and #Department of Physics, Reed College, Portland, Oregon 97202 USA

ABSTRACT A normal-mode and statistical mechanical calculation was carried out to determine the vibrational normal modes, contribution of internal fluctuations to the free energy, and hydrogen bond disruption of DNA triplex poly(dA) · 2poly(dT). The calculation was performed on both the x-ray fiber diffraction model with a N-type sugar conformation, and a newly proposed model with a S-type sugar conformation. Our calculated normal modes for the S-type structure are in better agreement with observed IR spectra for samples in D_2O solution. We also find that the contribution of internal fluctuations to free energy, premelting hydrogen bond disruption probability, and hydrogen bond melting temperatures for the Hoogsteen and Watson-Crick hydrogen bonds all show that the S-type structure is dynamically more stable than the N-type structure in a nominal solution environment. Therefore our calculation supports experimental findings that the triplex $d(T)_n \cdot d(A)_n d(T)_n$ most likely adopts a S-type sugar conformation in solution or at high humidity. Our calculations, however, do not preclude the possibility of an N-type conformation at lower humidities.

INTRODUCTION

The triple-stranded structures of DNA are of significant interest. Site-specific triplex formation has potential for therapy and genome mapping applications. Over the last few years many experimental studies have been carried out to measure the kinetics (Maher et al., 1990; Singerton and Dervan, 1993) and thermodynamics (Plum et al., 1990; Pilch et al., 1990; Manzini et al., 1990) of triplex formation, to analyze triplex conformation from vibrational spectroscopy (Howard et al., 1992; Quali et al., 1993; White and Powell, 1995; Dagneaux et al., 1995), to determine triplex structure from NMR (Radhakrishnan and Patel, 1994a) and x-ray crystallography (van Meervelt et al., 1995), and to study ligand-triplex binding (Mergny et al., 1992; Park and Breslauer, 1992; Durand et al., 1992; Lin and Patel, 1992). Several theoretical studies have also been carried out (Laughton and Neidle, 1992a,b; Raghunathan et al., 1993; Mohan et al., 1993; Cheng and Pettitt, 1995).

Despite this effort, there is very little detailed structural information currently available for triple helices. Arnott and co-workers determined the structure of poly(dA) · 2poly(dT) by x-ray fiber diffraction in 1974 (Arnott and Selsing, 1974). More recently, high-resolution x-ray crystal structural data have begun to emerge. However, these are triplet structures from protein-DNA complexes (Schultz et al., 1991; Luisi et al., 1991) and a DNA duplex-overlapping complex (van Meervelt et al., 1995). The fiber-diffraction model of Arnott and co-workers is still the only experimental model available for isolated DNA triplexes. This model shares structural features with A-form helices, including N-type (C3′-endo) sugar conformation and large negative x-displacement values. The NOE patterns (Radhakrishnan et al., 1992; Wang et al., 1992), the measured proton-proton scaler coupling constants (Macaya et al., 1992), and NMR solution structures (Radhakrishnan and Patel, 1994) are inconsistent with this assumption of an N-type sugar conformation. Marker bands characteristic of an S-type (C2′-endo) sugar conformation have been found in a number of infrared (IR) and Raman vibrational spectra (Thomas and Peticolas, 1983; Howard et al., 1992; Quali et al., 1993). In addition, a molecular mechanics study showed that B-conformation is energetically favored in DNA triplexes (Laughton and Neidle, 1992b). From these experimental and theoretical findings a new model of $d(T)_n \cdot d(A)_n d(T)_n$ with an S-type sugar conformation has been proposed, based on computer modeling (Raghunathan et al., 1993).

Given the limited structural data, we test available structures by theoretical modeling calculations to see whether these structures can give results in agreement with observations in solution. We report on a lattice dynamics calculation to determine the vibrational normal modes for both the N-type and the S-type model of poly(dA) · 2poly(dT) (an infinite triplex generated from the $d(T)_n \cdot d(A)_n d(T)_n$ structure). Our calculated normal-mode frequencies are compared with the observed vibrational spectrum to determine which structure has the better correlation. We further examine the dynamic stability of these structural models. A statistical mechanics calculation is carried out to determine and compare the contribution of internal thermal fluctuations to the free energy of the two models. The hydrogen bond (H-bond) disruption probabilities (which measure the likelihood of finding a particular H-bond being disrupted) in the two structures are also calculated and compared with

Received for publication 26 August 1996 and in final form 6 December 1996.

Address reprint requests to Dr. Y. Z. Chen, Department of Physics, Purdue University, West Lafayette, IN 47907-1396. Tel.: 317-494-8744; Fax: 317-494-0706; E-mail: yzchen@physics.purdue.edu.

0006-3495/97/03/1327/08 $2.00

observations. This calculation is carried out by using a microscopic statistical self-consistent approach we have developed to study DNA (Chen and Prohofsky, 1994) and drug-DNA complexes (Chen and Prohofsky, 1995a). Our H-bond disruption calculation corresponds to nominal physiological salt and solution condition. Nonstructured water enters into our calculations in terms of the proper choice of dielectric constants, the parameters of hydrogen bonds, and the assumption that all of the static force effects, including solvent, are automatically balanced at specific equilibrium positions.

The static energy of the two structural models considered in this work has been determined (Raghunathan et al., 1993). Therefore an analysis of the internal thermal fluctuation contribution to the free energy, along with the structural energy, can be used as a measure of the relative stability of the two structures. The disruption of hydrogen bonds connecting the bases is essential for both premelting base separation and melting of DNA. Another important factor is base-base stacking interactions. Although with a different backbone conformation, the stacking patterns of the two structures are very similar (Raghunathan et al., 1993). As a result, the base stacking energies should be similar in the two structures. Given the similar base stacking energies, the disruption probability of Hoogsteen and Watson-Crick hydrogen bonds can be used as another indicator of the dynamic stability of the triplex. In an earlier study of duplex DNA (Chen and Prohofsky, 1994) we found that our calculated hydrogen bond disruption probability shows a collective critical transition. This transition is associated with the onset of massive bond breaking, and it occurs near observed melting temperature. In the present work we find similar critical transitions for both Hoogsteen and Watson-Crick bonds. The temperatures of these critical transitions are compared to the temperatures of the observed biphasic melting of $d(T)_n \cdot d(A)_n d(T)_n$.

THEORETICAL METHODS

Structural models

The DNA triplexes studied in this work are two models of poly(dA) · 2poly(dT). Both models are a linear chain with infinite length. One model has an N-type sugar conformation and is generated from the x-ray fiber diffraction structure of Arnott and co-workers (Arnott and Selsing, 1974). The other model has an S-type sugar conformation and is generated from the model of $d(T)_n \cdot d(A)_n d(T)_n$ by Raghunathan and co-workers (Raghunathan et al., 1993). In these models no explicit hydrogen atoms are given. The masses and charges of these hydrogen atoms are added to their parent atoms.

Force fields and hydrogen bond parameters

The valence force constants for the DNA bases are from a DNA spectra study (Tsuboi et al., 1973), and those of the DNA backbones are from a separate refinement analysis (Lu et al., 1977). It should be noted that a new set of valence force constants for some of the DNA bases have been published (Tsuboi et al., 1987). The new force constants for adenine are from ab initio calculation, and they are not specifically refined to the observed spectrum. Moreover, no force constants for thymine are given. On the other hand, the old set of force constants was empirically fitted to the observed vibrational spectra and thus was more suitable for normal-mode analysis. Therefore in the present work the old set of force constants will be used. In addition to the valence force constants, we also incorporate base stacking and long-range Coulomb force interactions. These force constants are necessary to reproduce the observed acoustic modes (Mei et al., 1981) and were formulated in earlier studies (Mei et al., 1981; Prabhu et al., 1989). Both H-bond force constants and cross-strand base-base stacking force constants are allowed to change with temperature, as determined by the self-consistent calculations. Temperature-dependent H-bond force constants are calculated from a Morse potential that describes the effective potential between H-bonded atoms (Baird, 1974). The Morse parameters for the Watson-Crick H-bonds are the same as those we have used for duplex DNA (Chen and Prohofsky, 1993). The Morse parameters for the Hoogsteen H-bonds are given in Table 1. In Table 1 two sets of parameters are given; one set is calculated based on the S-type structure, and the other set based on the N-type structure. The calculated H-bond force constants are further scaled, taking into consideration the effect of disrupted bonds in the system (Chen and Prohofsky, 1994). The temperature behavior of the cross-strand base-base stacking force constants is approximated by scaling these force constants by relevant base disruption probability (Chen and Prohofsky, 1994).

TABLE 1 Morse parameters (a, r_0, and V_0), equilibrium bond length r_{eq} at 293 K, and maximum bond stretch length L_{max} of the Hoogsteen H-bonds in DNA triplex poly(dA) · 2poly(dT)

Structure	Bond	a (Å^{-1})	r_0 (Å)	V_0 (kcal/mol)	r_{eq} (Å)	L_{max} (Å)
S-type	N6-H-O4	2.042	2.761	3.156	2.932	3.232
	N7-H-N3	2.006	2.795	3.020	2.919	3.169
N-type	N6-H-O4	1.990	2.752	3.181	2.923	3.232
	N7-H-N3	1.950	2.822	2.865	2.948	3.169

The Morse potential is given as $V = V_0 (1 - \exp\{-a(r - r_0)\})^2 - V_0$, in which r is the distance between the two bond-end atoms.

Lattice dynamics calculation of vibrational normal modes

The detailed formulation of lattice dynamics for helical molecules has been given in earlier publications (Chen and Prohofsky, 1995b,c). The atomic-level normal-mode Hamiltonian for an infinite repeating helix can be given (Chen and Prohofsky, 1995b) by

$$H_0 = \sum_{n,i} \frac{1}{2} M_i \dot{\mathbf{u}}_{ni}^2 + \sum_k \sum_{n,m} \sum_j \frac{1}{2} \phi_{n-m,j,k} s_{n-m,j,k}^2, \quad (1)$$

where n and m are the indices of the repeating unit cells, i is the index of the atoms in a unit cell, j is the index for internal coordinates, and k specifies the types of harmonic motion (valence bond stretch, angle bending, torsion, out-of-plane bending, H-bonding, and motions induced by the nonbonded atom-atom van der Waals and Coulomb interactions). u_{ni} is the displacement of the ith atom in the nth unit cell in Cartesian coordinates, $s_{n-m,j,k}$ is the internal coordinate, and $\phi_{n-m,j,k}$ is the effective internal force constant for a particular bond motion. The force constants include a standard valence force field, hydrogen bond force constants, and a nonbonded force field including van der Waals and Coulomb interactions.

A potential energy distribution analysis (Letellier et al., 1986; Chen and Prohofsky, 1995c) is used to determine the character of a normal mode (i.e., the internal motion associated with that mode). The calculation was performed on an IBM RS6000 570 server using the IMSL Hermitian complex diagonalizations subroutine DEVCHF.

Statistical calculation of vibrational free energy and hydrogen bond disruption probability

We employ a microscopic statistical self-consistent approach to calculate the dynamic stability of both S-type and N-type poly(dA) · 2poly(dT). This calculation corresponds to physiological salt and solution conditions under which our force fields, potential parameters, and dielectric constants were fitted. The role of nonlocalized waters enters into our calculation in several ways. First, the system is assumed to be embedded in a dielectric solvent medium. Second, the parameters of the hydrogen bond potential are fitted to include the solvent and salt shielding effects at the nominal solvent salt condition. Third, all static force effects, including solvent, are automatically balanced by choosing specific equilibrium positions for each atom in the effective force approximation.

Our approach is derived from the self-consistent phonon theory of anharmonic lattice dynamics developed in the 1960s for the study of quantum crystals (Werthamer, 1970). This approach is based on the Bogoliubov variational theorem, which states that the free energy F of a system can be approximated by the solutions of an effective Hamiltonian H_{eff} (Callen, 1985). From the Bogoliubov inequality $F \leq F_{eff} + \langle H - H_{eff} \rangle$, one can self-consistently adjust the parameters of the trial Hamiltonian H_{eff} with respect to the true Hamiltonian H to find a trial system that minimizes the left-hand side terms and thus best approaches the true free energy. Here F_{eff} is the free energy of the trial Hamiltonian system. Both the free energies and Hamiltonians have two components, one static and one dynamic. The dynamic component is the internal thermal fluctuational vibrational energies, and it can be approximated by H_0 given in Eq. 1. The static component is the total potential at equilibrium positions. Therefore $H_{eff} = H_0 + V(r_{eq})$. The internal thermal fluctuational component of the free energy F^{ITF} can be approximated by F_{eff}, and it is given from the normal modes as

$$F^{ITF} = K_B T \sum_l \ln\left[2 \sinh\left(\frac{\hbar\omega_l}{2K_B T}\right)\right], \quad (2)$$

where ω_l and l are the frequency and the index of the normal modes, respectively. T is the temperature, k_B is Boltzmann's constant, and $\hbar$ is Planck's constant divided by 2π.

The self-consistent Bogoliubov approach gives rise to statistical probability distribution functions of finding a H-bond with a particular length. From these distribution functions one can determine the probability of finding a H-bond fluctuating beyond a certain breakdown point, i.e., the disruption probability of an individual H-bond. This probability is given by an integration over the distribution function:

$$P_j = \int_{L_j^{max}}^{\infty} dr e^{-(r-\langle r_j \rangle)^2/2\langle u_j^2 \rangle}, \quad (3)$$

where j is the index, $\langle u_j^2 \rangle$ is the mean vibrational square amplitude, and L_j^{max} is the maximum stretch length (breakdown point) of the H-bonds.

The probability P_j is a physical quantity measuring likelihood, the threshold of which represents hydrogen bond breaking ($P_j = 1$). This concept is needed in the use of unbounded potentials necessary for the ensemble used in statistical calculations involving many base pairs. Statistical mechanics is the only way to access the microsecond time scale of hydrogen bond disruption. The detailed description of the methodology can be found in our earlier publications (Chen and Prohofsky, 1994, 1995a). At temperatures below the onset of melting, the disruption of the individual H-bond can be regarded as independent event. As a result, the disruption probability of all Hoogsteen H-bonds P^{HG} and that of all Watson-Crick H-bonds $P^{W\text{-}C}$ in a triple-base unit can be given as the product of P_js:

$$P^{HG} = P_{N6(A1)-H-O4(T2)} \times P_{N7(A1)-H-N3(T2)}$$
$$P^{W-C} = P_{N6(A1)-H-O4(T1)} \times P_{N1(A1)-H-N3(T1)}. \quad (4)$$

RESULTS AND DISCUSSION

Vibrational normal modes and sugar conformation

Tables 2 and 3 list our calculated vibrational normal-mode frequencies in the region between 750 cm^{-1} and 1000 cm^{-1} for S-type and N-type poly(dA) · 2poly(dT), respectively. For comparison, the observed IR frequencies for $(dT)_n \cdot (dA)_n(dT)_n$ in D_2O solution (Howard et al., 1992; Liquier et al., 1991) are included. In these tables only those modes that would appear in the IR spectra are given. The internal motion associated with the normal modes at medium- and high-frequency regions (>500 cm^{-1}) can be determined by a potential energy distribution (PED) analysis (Letellier et al., 1986; Chen and Prohofsky, 1995c). From this analysis the internal bond motion with the largest PED values is identified as the motion associated with that normal mode. The calculated largest PED for each normal mode is listed in Tables 2 and 3. As expected, the modes in this frequency region correspond primarily to localized motions in the sugar-phosphate backbone in both Watson-Crick duplex and the third strand.

From Tables 2 and 3 we find fair agreement between observed IR frequencies and our calculated normal modes for the S-type structure. In contrast to the fair agreement for the S-type structure, a large discrepancy is found between several observed IR frequencies and calculated normal modes for the N-type structure, as shown in Table 3. We are unable to assign observed modes at 945.5 and 861 cm^{-1} to any calculated mode. In addition, a significant frequency difference is found between calculated modes and observed modes at 972.5 and 792 cm^{-1}. We are unable to find a mode with c1′-c2′-c3′ character to match the observed mode at 770 cm^{-1}. This observed mode is tentatively assigned in Table 3 to the calculated modes with c4′-o4′-c1′ character. A large discrepancy is again found between the observed 770 cm^{-1} mode and the tentatively assigned mode.

All of the observed modes in this frequency region are associated with localized vibrational motion in the sugar-phosphate backbone. These observed modes are for samples in D_2O solution. Therefore the fair agreement for the S-type structure and the poor agreement for the N-type structure indicate that the backbone of the triplex DNA (dT) · (dA)(dT) most likely adopts the S-type sugar conformation in solution. This conclusion is consistent with results from other research groups, which showed that the solution vibrational spectra of DNA triplexes contain S-type marker bands (Thomas and Peticolas, 1983; Howard et al., 1992; Quali et al., 1993). It is also consistent with studies of NOE patterns (Radhakrishnan et al., 1992; Wang et al., 1992), proton-proton scaler coupling constants (Macaya et al., 1992), and NMR structural analysis (Radhakrishnan and Patel, 1994a) in solution.

In this work observed IR bands for samples in D_2O solution are used to compare with our calculations. The effect associated with deuteration of the bases may affect some of the observed D_2O bands. For instance, the 861-cm^{-1} band is known to be affected by deuterated thymines, which results in the shift of frequency from 861 cm^{-1} to 870 cm^{-1}. This has prompted a suggestion to use samples in H_2O instead of D_2O to evaluate the ratio of S- and N-type sugars. A comparison of the D_2O spectrum with that at 92% RH (to be published) shows that such a frequency shift occurs only in a few bands in this region. Hence the effect of base deuteration does not affect our conclusion.

NMR studies have shown that the three strands of a noncanonical triplex can adopt different types of sugar puckers (Radhakrishnan and Patel, 1994c). Although vibrational spectroscopy can reveal bands associated with each of these pucker conformations, it may not be used as an infallible guide to uniquely determine the structure. Introduction of isotopic labels is useful for solving this problem (Surewicz et al., 1993). In addition, the use of other modes, such as P-O stretch, in the backbone is also helpful. Moreover, a combined analysis of free energy and stability can serve as double check.

Vibrational normal modes involve excitations in chemical bonds in all three strands, which makes it difficult to unequivocally distinguish between various models with minor differences in different strands. It is worth noting that a local conformation change can effect the distribution of vibrational potential energy in that region. As a result,

TABLE 2 Calculated normal-mode frequencies ω_S^{theor} for the S-type triplex poly(dA) · 2poly(dT) in the region between 750 cm^{-1} and 1000 cm^{-1}

	Calculation			
IR ω^{expt} (cm^{-1})	ω_S^{theor} (cm^{-1})	$\Delta\omega_S$ (cm^{-1})	Assignment (PED %)	Residue
972.5	977.2	4.7	c2′-c3′ (14.6), c5-Me (7.1), c1′-n1 (6.6)	T2
945.5	951.5	6.0	c4′-c5′ (7.3), o4′-c1′ (6.5), c6-n6 (6.2)	A1
899.5	895.3	−4.2	o5-p (23.7), o3-p (17.0), o3-c3′-c4′ (7.6)	T1, A1
870.0	874.6	4.6	c2′-c3′ (16.0), c1′-c2′ (10.9), o3-c3′-c4′ (8.5)	T2
840.5	847.2	6.7	o5-p (10.0), c2′-c3′ (6.3), c3′-c4′ (6.1)	A1, T1
792.0	797.9	5.9	o3-p (36.0), o5-p (15.4), c4′-c5′ (5.4)	T1, A1, T2
770.0	763.6	−6.4	c1′-c2′-c3′ (13.9), c3′-c4′ (6.0), c5-Me (5.5)	T1

ω^{expt} is the observed IR frequency for $d(T)_n \cdot d(A)_nd(T)_n$ in D_2O solution (Howard et al., 1992). $\Delta\omega_S = \omega_S^{theor} - \omega^{expt}$. Only those modes observed in the IR spectrum are listed. A1 and T1 are the nomenclature for the Watson-Crick adenine and thymine base and T2 for the third-strand thymine base. The estimated standard deviation, $\sigma_S = \sqrt{\Sigma_i(\Delta\omega_S)_i^2/n}$, is found to be 5.57 cm^{-1}.

TABLE 3 Calculated normal-mode frequencies ω_N^{theor} for the N-type triplex poly(dA) · 2poly(dT) in the region between 750 cm^{-1} and 1000 cm^{-1}

	Calculation			
IR ω^{expt} (cm^{-1})	ω_N^{theor} (cm^{-1})	$\Delta\omega_N$ (cm^{-1})	Assignment (PED %)	Residue
972.5	952.3	−20.2	c2′-c3′ (23.4), c1′-c2′ (8.5), c3′-c4′ (6.0)	T2
945.5				
899.5	893.5	−6.0	o5-p (21.8), o3-p (13.0), o3-c3′-c4′ (9.1)	T1, A1
870.0				
840.5	842.4	1.9	o5-p (12.8), o3-p (12.4), c4′-o4′ (6.6)	A1
792.0	823.3	31.3	o3-p (45.6), c4′-o4′ (7.8), c1′-c2′ (5.4)	T2, A1, T1
770.0	727.8	−42.2	c4′-o4′-c1′ (9.9), o4′-c1′-c2′ (9.9), c1′-c2′-c3′ (6.6)	T1

ω^{expt} is the observed IR frequency for $d(T)_n \cdot d(A)_n d(T)_n$ in D_2O solution (Howard et al., 1992). $\Delta\omega_N = \omega_N^{theor} - \omega^{expt}$. Only those modes observed in the IR spectrum are listed. A1 and T1 are the nomenclature for the Watson-Crick adenine and thymine base and T2 for the third-strand thymine base. The estimated standard deviation, $\sigma_N = \sqrt{\Sigma_i(\Delta\omega_S)_i^2/n}$, is found to be 25.21 cm^{-1}.

modes with strong local character emerge. These modes may be useful in distinguishing different models based on comparison between these modes and the observed spectrum. In addition, isotopically enhanced vibrational spectroscopy can also be explored to deal with this problem.

The present work deals with a canonical Y · RY triplex in which all of the sugars adopt one pucker type. In general, most sugars in a canonical Y · RY triplex adopt one pucker type (Radhakrishnan and Patel, 1994b). Therefore it is relatively easy to compare structural models of these triplexes based on sugar pucker and phosphate group normal modes.

Contribution of internal thermal fluctuations to free energy

The contribution of internal thermal fluctuations to the free energy F^{ITF} of both the S-type and the N-type model as a function of temperature is given in Fig. 1. We find that at temperatures below 319 K the F^{ITF} of the S-type structure is smaller than that of the N-type structure. The relative stability of the S-type and the N-type triplex in solution depends on the free energy difference. This difference has an internal component and a contribution from the solvent. The internal component consists of a static part and a dynamic part. The static part is the energy difference between the two structures at their respective potential minima. The dynamic part is the fluctuational thermal motion contribution to the free energy. A CHARMM molecular mechanics calculation (Raghunathan et al., 1993) has shown that the total static energy of the S-type structure is lower than that of the N-type structure. As pointed out earlier in the present paper, our calculation includes the solvent effect in terms of dielectric medium, the parameters of hydrogen bonds, and the assumption that all of the static force effects, including solvent, are automatically balanced at specific equilibrium positions. Therefore our calculation of a lower F^{ITF} for the S-type structure further indicates that the S-type structure is likely to be more stable in solution. This result is also consistent with the conclusion from our normal-mode calculation that the S-type structure gives results that are in better agreement with experiments.

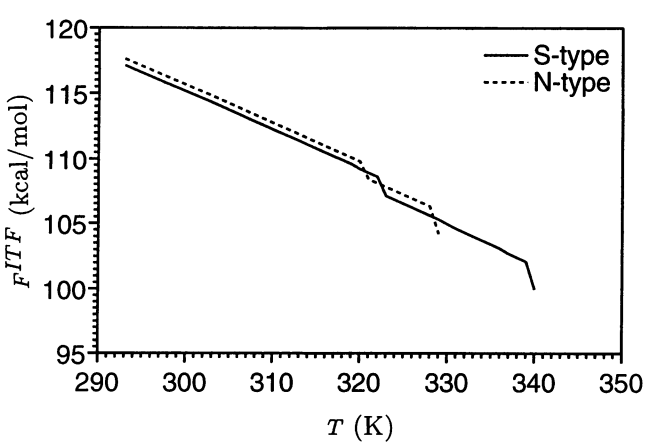

FIGURE 1 The contribution of internal thermal fluctuations to the free energy F^{ITF} of both the S-type and the N-type model of triplex poly(dA) · 2poly(dT) as a function of temperature.

From Fig. 1 we find abrupt changes in the F^{ITF} curves at certain critical temperatures. These abrupt changes are related to massive disruption of the Hoogsteen and Watson-Crick H-bonds, which will be discussed later in the paper. There are two abrupt changes in each F^{ITF} curve. The one at lower temperature corresponds to the massive disruption of Hoogsteen H-bonds, and that at higher temperature corresponds to the massive disruption of Watson-Crick H-bonds. For the N-type structure, massive disruption of the Hoogsteen and Watson-Crick H-bonds occurs at 319 K and 327 K, respectively. For the S-type structure, the massive disruption of both Hoogsteen and Watson-Crick H-bonds occurs at a higher temperature than that of the N-type structure, which is at 322 K and 338 K, respectively.

A recent molecular mechanics calculation (Cheng and Pettitt, 1995) of several models of triplex $d(T)_7 \cdot d(A)_7 d(T)_7$ with different solvent models showed that the relative free energy of the model with all B-type backbones is higher than that of the model with all A-type backbones. That result, however, is not necessarily in conflict with our calculation and the result by Raghunathan et al. (1993).

Both the A-type and B-type models considered in Cheng and Pettitt's study are different from those considered in this work and in the work by Raghunnathan et al. Based on the same initial structure, Cheng and Pettitt derived an A-type model with backbone torsion angles that differed by as much as 10–20° from those in Arnott's N-type structure. Their B-type model was generated from an initial structure with standard B-conformation. The backbone torsion angles of this model differ from those of the S-type model used in the present work by as much as 40°. In addition, the average helical rise and twist angle of their B-type (3.0 Å, 32.5°) and A-type (3.0 Å, 31.5°) models are also different from those (3.26 Å, 30.0°) of the models used in the present work. Such differences in backbone torsion angles and helical parameters are expected to result in differences in the calculated relative energies between the models of Cheng and Pettitt and the models used in the present work.

Hydrogen bond disruption

We have calculated the disruption probability of individual H-bonds in both the S-type and the N-type model using the statistical method we have developed (Chen and Prohofsky, 1994). There are two Hoogsteen H-bonds in the system. The stability of this bonding can be measured by a quantity P^{HG}, the disruption probability of all Hoogsteen H-bonds in a triple-base unit, which is the product of the disruption probability of the individual Hoogsteen H-bonds. Likewise, the disruption probability of all Watson-Crick H-bonds in a triple-base unit $P^{W\text{-}C}$ is the product of disruption probability of the two Watson-Crick H-bonds in the system. The calculated P^{HG} and $P^{W\text{-}C}$ for both the S-type and the N-type structure as a function of temperature are given in Fig. 2. We find that at all temperatures both P^{HG} and $P^{W\text{-}C}$ of the S-type structure are smaller than those of the N-type structure. This shows that both Hoogsteen H-bonding and Watson-Crick bonding in the S-type structure are more stable than in the N-type structure. Thus from the perspective of H-bonding stability, the S-type structure is more stable than the N-type structure. Such a result is consistent with both free-energy and normal-mode calculations, as discussed earlier in this paper.

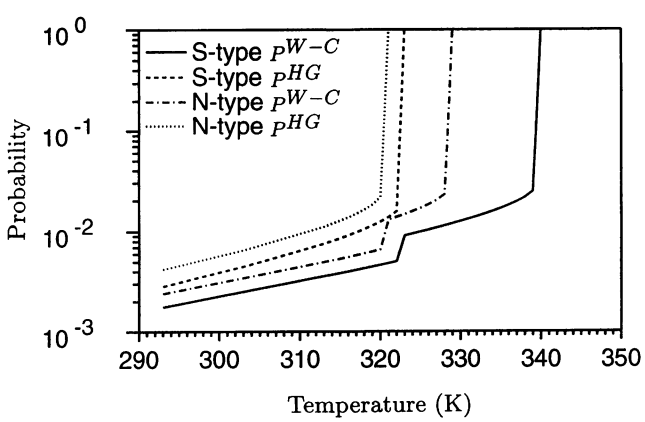

FIGURE 2 Disruption probability of all Hoogsteen H-bonds P^{HG} and that of all Watson-Crick H-bonds $P^{W\text{-}C}$ in a triple base unit of both the S-type and the N-type model of triplex poly(dA) · 2poly(dT) as a function of temperature.

From Fig. 2 we find that both the P^{HG} and the $P^{W\text{-}C}$ curves show critical behavior at certain critical temperatures. Each of the two P^{HG} curves shows a dramatic increase from $\sim 10^{-2}$ to ~ 1 at the critical temperature of 321 K for the N-type structure and 323 K for the S-type structure. This critical behavior is indicative of the onset of massive Hoogsteen bond disruption melting, and the corresponding critical temperature can be defined as the Hoogsteen H-bond melting temperature T_m^{HG}. Two critical transitions can be seen in each of the two $P^{W\text{-}C}$ curves. The first transition involves a sudden increase in $P^{W\text{-}C}$ at T_m^{HG}, and this reduced Watson-Crick H-bond stability is induced by the massive disruption of the Hoogsteen H-bonds. The second transition involves a dramatic increase in $P^{W\text{-}C}$ from $\sim 10^{-2}$ to ~ 1, and it again indicates massive disruption of Watson-Crick H-bonds. Therefore we can define the critical temperature of the second transition as the Watson-Crick H-bond melting temperature $T_m^{W\text{-}C}$. The $T_m^{W\text{-}C}$ for the N-type and S-type structures is 329 K and 340 K, respectively.

In our earlier studies of duplex DNA (Chen and Prohofsky, 1994) we have found that our calculated H-bond melting temperatures correlate quite well with the observed melting temperatures for various DNA duplex sequences. This indicates that hydrogen bond melting may be used as a good indicator of helix-coil transition. It is therefore of interest to compare our calculated T_m^{HG}s and $T_m^{W\text{-}C}$s with the observed triplex-duplex transition temperature and duplex-transition temperature of poly(dA) · 2poly(dT) (Pilch et al., 1990; Park and Breslauer, 1992). The comparison is given in Table 4. Also included in Table 4 is the calculated and observed melting temperature difference $\Delta T_m = T_m^{W\text{-}C} - T_m^{HG}$. It should be pointed out that experimental ultraviolet (UV) measurements were carried out at different salt conditions. Both T_m^{HG} and $T_m^{W\text{-}C}$ are dependent on salt concentration. It is not surprising, therefore, that observed values from one experiment differ from those of another. Because T_m^{HG} and $T_m^{W\text{-}C}$ are measured at the same salt condition, the ΔT_m is insensitive to salt concentration, as shown in Table 4. We find that our calculated ΔT_m for the S-type structure is in good agreement with observations. On the other hand, the ΔT_m for the N-type structure is substantially different from observed values. In addition, the calculated T_m^{HG} and $T_m^{W\text{-}C}$ for the S-type structure are in fair agreement with observed values from one experiment. In contrast, the calculated $T_m^{W\text{-}C}$ for the N-type model is substantially different from the observed value. This result again indicates that the S-type structure is in better agreement with experiments.

The close correlation between calculated T_m^{HG} and $T_m^{W\text{-}C}$ and observed triplex-duplex and helix-coil transition temperatures indicates that hydrogen bond melting can be used as an indicator of triplex-duplex transition as well as helix-coil transition. It is interesting to compare our calculated temperature behavior of P^{HG} and $P^{W\text{-}C}$ with an observed

TABLE 4 Calculated Hoogsteen H-bond melting temperature T_m^{HG} and Watson-Crick H-bond melting temperature T_m^{W-C} for both S-type and N-type triplex poly(dA) · 2poly(dT)

System	Method	T_m^H (K)	T_m^{WC} (K)	ΔT_m (K)
S-type poly(dA) · 2poly(dT)	Theory	323	340	17
N-type poly(dA) · 2poly(dT)	Theory	321	329	8
Poly(dA) · 2poly(dT)*	UV	325	343	18
Poly(dA) · 2poly(dT)#	UV	341	354	13

For comparison, the observed triplex-duplex transition temperature and the helix-coil transition temperature are also included. $\Delta T_m = T_m^{W-C} - T_m^{HG}$, and observed values are from *Pilch et al. (1990) and #Park and Breslauer (1992).

UV melting curve. The UV absorbance arises from the π-π^* electronic transition in both purine and pyrimidine bases. An increase in the absorbance reflects a change in base stacking. In a triple-base unit there are two Watson-Crick bases and one third-strand base. Assuming that H-bond disruption facilitates base unstacking, the observed UV curve may be compared to a temperature-dependent curve of the average disruption probability of a triple-base unit, $\langle P\rangle = (2P^{W\text{-}C} + P^{HG})/3$. The $\langle P\rangle$ is shown in Fig. 3 as a function of temperature. We find that the curve indeed shows a biphasic transition very similar to that of the observed UV curves for $(dT)_n \cdot (dA)_n(dT)_n$ (Pilch et al., 1990; Park and Breslauer, 1992).

CONCLUSION

Structural features of molecules can be revealed from high-frequency vibrational normal modes because the energy of these modes tends to localize in particular bonds and is sensitive to the structure of molecules. An analysis of two models of DNA triplex poly(dA) · 2poly(dT) shows that the normal modes of the model with an S-type sugar conformation are in better agreement with observed IR frequencies. Large discrepancies are found between the normal modes of the model with an N-type sugar conformation and observed IR frequencies. Therefore the S-type structure seems to better describe the structure of poly(dA) · 2poly(dT) in solution or at high humidity.

The dynamic fluctuations of molecules around their average conformations play an important role in the stability and function of these molecules. A microscopic self-consistent statistical calculation is carried out to determine the dynamic stability of the two structural models of poly(dA) · 2poly(dT). The internal thermal fluctuational free energy of the S-type model is found to be smaller than that of the N-type model. In addition, both the Hoogsteen and Watson-Crick hydrogen bonding in the S-type model is more stable than that in the N-type model at temperatures from room temperature to melting temperature. As revealed by other researchers, the stacking interactions in these two structures are very similar. All of these results, together with results from other researchers' molecular mechanics calculations, indicate that the S-type structure is more stable, at least in a high-humidity environment. This conclusion is consistent with our normal-mode analysis and with many other experimental findings.

Our calculations, however, do not preclude the possibility that the triplex poly(dA) · 2poly(dT) can adopt an N-type sugar conformation at lower humidities. Our dynamic stability calculations are suitable for a nominal salt and solution environment, as the parameters are refined from the data under these conditions. A recent experiment has shown hydration-dependent conformation changes in $G_{20} \cdot G_{20}C_{20}$ (White and Powell, 1995). The extensive simulation studies of Cheng and Pettitt (1995) also demonstrate the dependence of conformation on environment.

The combined vibrational spectroscopy, normal-mode, and statistical mechanical calculations used in analyzing the structure and dynamics of DNA triplex as presented in this work have broad applications in the analysis of other biomolecules and biomolecular assemblies. A homology strategy based on these techniques may be useful in conformation prediction and deformation analysis.

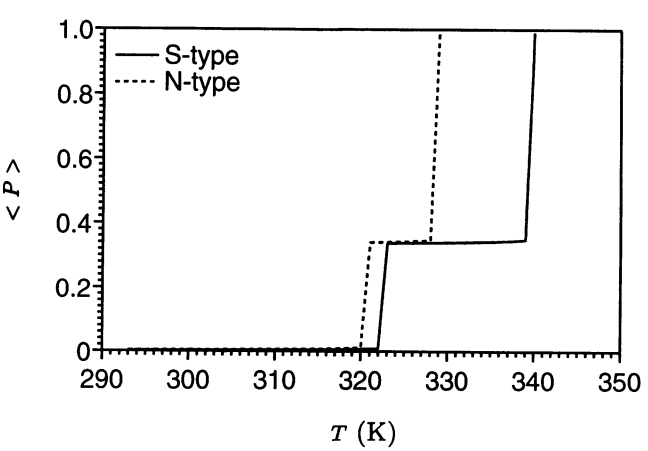

FIGURE 3 Average disruption probability $\langle P\rangle = (2P^{W\text{-}C} + P^{HG})/3$ of a triple base unit of both the S-type and the N-type model of triplex poly(dA) · 2poly(dT) as a function of temperature.

We thank the referees for valuable suggestions.

This work is supported in part by ONR grant N00014-92-K-1232 to YZC and EWP, and a grant to Reed College (JWP) under the Howard Hughes Medical Institute Undergraduate Biological Sciences Initiative.

REFERENCES

Arnott, S., and E. Selsing. (1974). Structures for the polynucleotide complexes poly(dA) · poly(dT) and poly(dT) · poly(dA) · poly(dT). *J. Mol. Biol.* 88:509–521.

Baird, N. C. 1974. Simulation of hydrogen bonding in biological systems: ab initio calculations for NH_3-NH_3 and NH_3-NH_4^+. *Int. J. Quantum Chem. Quantum Biol. Symp.* 1:49–54.

Callen, 1985. Thermodynamics and an Introduction to Thermostatics, 2nd Ed. Wiley and Sons, New York. 433–435.

Chen, Y. Z., and E. W. Prohofsky. 1993. Differences in melting behavior between homopolymers and copolymers of DNA: role of non-bonded forces for GC and the role of the hydration spine and premelting transition for AT. *Biopolymers.* 33:797–812.

Chen, Y. Z., and E. W. Prohofsky. 1994. Near-neighbor effects in cooperative modified self-consistent phonon approximation melting in DNA. *Phys. Rev.* E49:873–881.

Chen, Y. Z., and E. W. Prohofsky. 1995a. Calculation of the dynamics of drug binding in a netropsin-DNA complex. *Phys. Rev.* E51:5048–5058.

Chen, Y. Z., and E. W. Prohofsky. 1995b. Sequence and temperature dependence of the interbase hydrogen bond breathing modes in B-DNA polymers. Comparison with low frequency Raman peaks and their role in helix melting. *Biopolymers.* 35:573–583.

Chen, Y. Z., and E. W. Prohofsky. 1995c. Normal mode calculation of a netropsin-DNA complex: effect of structural deformation on vibrational spectrum. *Biopolymers.* 35:657–667.

Cheng, Y. K., and B. M. Pettitt. 1995. Solvent effects on model $d(CG \cdot G)_7$ and $d(TA \cdot T)_7$ DNA triple helices. *Biopolymers.* 35:457–473.

Dagneaux, C., J. Liquier, and E. Taillandier. 1995. Sugar conformations in DNA and RNA-DNA helices determined by FTIR spectroscopy: role of backbone composition. *Biochemistry.* 34:16618–16623.

Durand, M., N. T. Thuong, and J. C. Maurizot. 1992. Binding of netropsin to a DNA triple helix. *J. Biol. Chem.* 267:24394–24399.

Howard, F. B., H. T. Miles, K. Liu, J. Frazier, G. Raghunathan, and V. Sasisekharan. 1992. Structure of $d(T)_n \cdot d(A)_n \cdot d(T)_n$: the DNA triple helix has B-form geometry with C2′-endo sugar pucker. *Biochemistry.* 31:10671–10677.

Laughton, C. A., and S. Neidle. 1992a. Molecular dynamics simulation of the DNA triplex $d(TC)_5 \cdot d(GA)_5 \cdot d(C^+T)_5$. *J. Mol. Biol.* 223:519–529.

Laughton, C. A., and S. Neidle. 1992b. Prediction of the structure of the $Y^+ \cdot R^- \cdot R^+$-type DNA triple helix by molecular modelling. *Nucleic Acids Res.* 20:6535–6541.

Letellier, R., M. Ghomi, and E. Taillandier. 1986. Interpretation of DNA vibration modes. I. The guanosine and cytidine residues involved in poly(dG-dC) · poly(dG-dC) and $d(CG)_3 \cdot d(CG)_3$. *J. Biomol. Struct. Dyn.* 3:671–687.

Lin, C. H., and D. J. Patel. 1992. Site-specific covalent duocarmycin A-intramolecular DNA triplex complex. *J. Am. Chem. Soc.* 114: 10658–10660.

Liquier, J., P. Coffinier, M. Firon, and E. Taillandier. 1991. Triple helical polynucleotidic structures: sugar conformations determined by FTIR spectroscopy. *J. Biomol. Struct. Dyn.* 9:437–445.

Lu, K. C., E. W. Prohofsky, and L. L. Van Zandt. 1977. Vibrational modes of A-DNA, B-DNA, and A-RNA backbones: an application of a Green-function refinement procedure. *Biopolymers.* 16:2491–2506.

Luisi, B. F., W. X. Xu, Z. Otwinowski, L. P. Freeman, K. R. Yamamoto, and P. B. Sigler. 1991. Crystallographic analysis of the interaction of the glucocorticoid receptor with DNA. *Nature.* 352:497–505.

Macaya, R., E. Wang, P. Schultze, V. Sklenar, and J. Feigon. 1992. Proton nuclear magnetic resonance assignments and structural characterization of an intramolecular DNA triplex. *J. Mol. Biol.* 225:755–773.

Maher, L. J., P. B. Dervan, and B. Wold. 1990. Kinetic analysis of oligodeoxyribonucleotide-directed triple-helix formation on DNA. *Biochemistry.* 29:8820–8826.

Manzini, G., L. E. Xodo, D. Gasparotto, F. Quadrifoglio, G. A. van der Marel, and J. H. van Boom. 1990. Triple helix formation by oligopurine-oligopyrimidine DNA fragments. *J. Mol. Biol.* 213:833–843.

Mei, W. N., M. Kohli, E. W. Prohofsky, and L. L. Van Zandt. 1981. Acoustic modes and nonbonded interactions of the double helix. *Biopolymers.* 20:833–852.

Mergny, J. L., G. Duval-Valentin, C. H. Nguyenm, L. Perrouault, B. Faucon, M. Rougee, T. M. Garestier, E. Bisagni, and C. Helene. 1992. *Science.* 256:1681–1684.

Nishimura, Y., M. Tsuboi, S. Kato, and K. Morokuma. 1982. *In* Raman Spectroscopy, Linear and Nonlinear. J. Lascombe and V. Huong, editors. 703–725.

Mohan, V., P. E. Smith, and B. M. Pettitt. 1993. Evidence for a new spine of hydration: solvation of DNA triple helices. *J. Am. Chem. Soc.* 115: 9297–9298.

Park, Y. W., and K. J. Breslauer. 1992. Drug binding to higher ordered DNA structures: netropsin complexation with a nucleic acid triple helix. *Proc. Natl. Acad. Sci. USA.* 89:6653–6657.

Pilch, D. S., R. Brousseau, and R. H. Shafer. 1990. Thermodynamics of triple helix formation: spectrophotometric studies on the $d(A)_{10} \cdot 2d(T)_{10}$ and $d(C_3^+T_4C_3^+) \cdot d(G_3A_4G_3) \cdot d(C_3T_4C_3)$ triple helices. *Nucleic Acids Res.* 18:5743–5750.

Plum, G. E., Y. W. Park, S. F. Singerton, and P. B. Dervan. 1990. Thermodynamic characterization of the stability and the melting behavior of a DNA triplex: a spectroscopic and calorimetric study. *Proc. Natl. Acad. Sci. USA.* 87:9436–9440.

Prabhu, V. V., L. Young, E. W. Prohofsky, and G. S. Edwards. 1989. Hydrogen-bond melting in B-DNA copolymers in a mean-field self-consistent phonon theory. *Phys. Rev.* B39:5436–5443.

Quali, M., R. Letellier, F. Adnet, J. Liquier, J. S. Sun, R. Lavery, and E. Taillandier. 1993. A possible family of B-like triple helix structures: comparison with Arnott A-like triple helix. *Biochemistry.* 32: 2098–2103.

Radhakrishnan, I., and D. J. Patel. 1994a. Solution structure and hydration patterns of a prrimidine · purine · pyrimidine DNA triplex containing a novel T · CG base-triple. *J. Mol. Biol.* 241:600–619.

Radhakrishnan, I., and D. J. Patel. 1994b. DNA triplexes: solution structures, hydration sites, energetics, interactions, and functions. *Biochemistry.* 33:11405–11416.

Radhakrishnan, I., and Patel, D. J. 1994c. Solution structure of a prrimidine · purine · pyrimidine DNA triplex containing T · AT, C^+ · CG and G · TA triplexes. *Structure.* 2:17–32.

Radhakrishnan, I., D. J. Patel, and X. Gao. 1992. Three-dimensional homonuclear NOESY-TOCSY of an intramolecular pyrimidine · purine · pyrimidine DNA triplex containing a central G · TA triple: nonexchangeable proton assignments and structural implications. *Biochemistry.* 31:2514–2523.

Raghunathan, G., H. T. Miles, and V. Sasisekharan. 1993. Symmetry and molecular structure of a DNA triple helix: $d(T)_n \cdot d(A)_n \cdot d(T)_n$. *Biochemistry.* 32:455–462.

Schultz, S. C., G. C. Shields, and T. A. Steitz. 1991. Crystal structure of a CAP-DNA complex: the DNA is bent by 90°. *Science.* 253:1002–1007.

Surewicz, W. K., H. H. Mantsch, and D. Chapman. 1993. Determination of protein secondary structure by Fourier transform infrared spectroscopy: a critical assessment. *Biochemistry.* 32:389–394.

Singerton, S. F., and P. B. Dervan. 1993. Equilibrium association constants for oligonucleotide-directed triple helix formation at single DNA sites: linkage to cation valence and concentration. *Biochemistry.* 32: 13171–13179.

Thomas, G. A., and W. L. Peticolas. 1983. Fluctuations in nucleic acid conformations. 2. Raman spectroscopic evidence of varying ring pucker in A-T polynucleotides. *J. Am. Chem. Soc.* 105:993–996.

Tsuboi, M., S. Takahashi, and I. Harada. 1973. Infrared and Raman spectra of nucleic acids—vibrations in the base-residues. *In* Physico-Chemical Properties pf Nucleic Acids, Vol. 2. J. Duchesne, editor. 91–145.

Tsuboi, M., Y. Nishimura, A. Y. Hirakawa, and W. L. Peticolas. 1987. Resonance Raman spectroscopy and normal modes of nucleic acid bases. *In* Biological Applications of Raman Spectroscopy, Vol. 2. T. Spiro, editor. 109–179.

van Meervelt, L., D. Vlieghe, A. Dautant, B. Gallois, G. Precigoux, and O. Kennard. 1995. High-resolution structure of a DNA helix forming (C · G)G base triplets. *Nature.* 374:742–744.

Wang, E., S. Malek, and J. Feigon. 1992. Structure of a G · T · A triplet in an intramolecular DNA triplex. *Biochemistry.* 31:4838–4846.

White, A. P., and J. W. Powell. 1995. Observation of the hydration-dependent conformation of the $(dG)_{20} \cdot (dG)_{20}(dC)_{20}$ oligonucleotide triplex using FTIR spectroscopy. *Biochemistry.* 34:1137–1142.